Contents lists available at ScienceDirect

Chemical Engineering Research and Design

journal homepage: www.elsevier.com/locate/cherd

Small-scale experiments on stabilizing riser slug flow

Heidi Sivertsen[1], *Espen Storkaas*[2], *Sigurd Skogestad*[*]

Department of Chemical Engineering, Norwegian University of Science and Technology, Trondheim, Norway

A B S T R A C T

This paper describes the study and results from a small-scale lab rig, build to test different riser slug control strategies without the huge costs involved in larger scale experiments. Earlier experiments on this small-scale rig have shown that it was possible to stabilize the flow using a PI controller with a pressure measurement located upstream the riser base as measurement (Sivertsen and Skogestad, 2005).

During these earlier experiments, the slug flow behaved a bit differently from that observed in larger facilities. Instead of severe slugs where the gas entered the riser, the gas was released as Taylor bubbles. As one Taylor bubble managed to enter the riser, several more would quickly follow as the pressure drop across the riser decreased. To get a slug flow pattern that was closer to severe slugs, the length of the riser and the size of the gas buffer tank were increased. After implementing this new equipment, the slug flow regime resembled more the severe slugs seen in larger rigs. The aim now was to control the flow using only topside measurements and to compare with results found using upstream measurements.

A controllability analysis was performed in order to screen the different measurement candidates using a model developed by Storkaas et al. (2003). The analysis showed that it should be possible to control the flow using only topside measurements. The results from this analysis were then used as a background for the experiments performed in the lab.

The experimental results were successful. They showed that it was possible to control the flow and the results were actually better than predicted from the analysis. In fact, the results are comparable with the results obtained when using a pressure measurement upstream the riser (subsea measurement).

Keywords: Process control; Multiphase flow; Dynamic simulation; Petroleum; Riser slugging; Controllability analysis

1. Introduction

The behavior of multiphase flow in pipelines is of great concern in the offshore oil and gas industry, and a lot of time and effort have been spent studying this phenomena. The reason for this is that by doing relatively small changes in operating conditions, it is possible to change the flow behavior in the pipelines drastically. This has a huge influence on important factors such as productivity, maintenance and safety. Fig. 1 shows different flow regimes that can develop in an upward pipeline.

Some operating conditions lead to an undesirable slug flow regime that may cause severe problems for the receiving facilities due to varying flow rates and pressure in the system. This usually happens at the end of the life cycle of a well, when flow rates are lower than the system was designed for.

Being able to avoid slug flow in the pipeline is of great economic interest. For this reason it is important to be able to predict the flow regime before production starts, so that the problems can be taken care of as soon as they arise. Traditionally flow maps as the one in Fig. 2 have been produced as a tool to predict the flow regime that will develop in a pipeline (Taitel and Dukler, 1976; Barnea, 1987; Hewitt and Roberts, 1969). These maps show that the flow regime in a pipeline is highly dependent on the incoming superficial flow rates of gas (u_{GS}) and oil (u_{LS}).

[*] *Corresponding author.*
E-mail address: skoge@chemeng.ntnu.no (S. Skogestad).
Received 17 July 2008; Received in revised form 28 July 2009; Accepted 12 August 2009
[1] Current affiliation: StatoilHydro, EPN ONO ASG SMB PTC, Stjørdal, Norway.
[2] Current affiliation: ABB OG&P, Advanced Solutions, Oslo, Norway.
0263-8762/$ – see front matter
doi:10.1016/j.cherd.2009.08.007

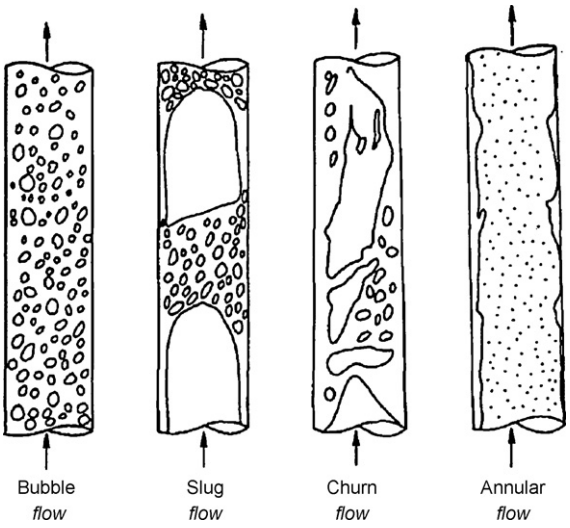

Fig. 1 – Vertical flow regime map of Taitel et al. (1980).

Even though the system is designed to avoid such problems in the earlier years of production, the production rate is changed during the production lifetime and problems can arise later on. Note however that these flow maps represent the "natural" flow regimes, observed when no feedback control is applied.

There exist different types of slugs, depending on how they are formed. They can be caused by hydro-dynamical effects or terrain effects. The slugs can also be formed due to transient effects related to pigging, start-up and blow-down and changes in pressure or flow rates.

Hydrodynamic slugs are formed by liquid waves growing in the pipeline until the height of the waves is sufficient to completely fill the pipe. These slugs can melt together to form even larger slugs and occur over a wide range of flow conditions.

Terrain slugging is caused by low-points in the pipeline topography, causing the liquid to block the gas until the pressure in the compressed gas is large enough to overcome the hydrostatic head of the liquid. A long liquid slug is then pushed in front of the expanding gas upstream. One example of such a low-point is a subsea line with downwards inclination ending in a vertical riser to a platform. In some cases the entire riser can be filled with liquid until the pressure in the gas is large enough to overcome the hydrostatic pressure of the

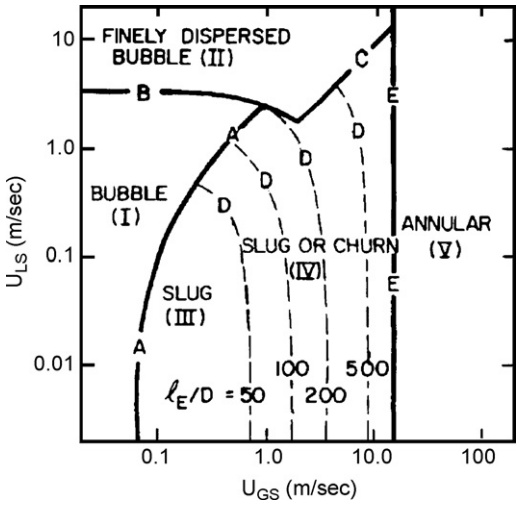

Fig. 2 – Flow regime map for 25 mm diameter vertical tubes, air–water system (Taitel et al., 1980).

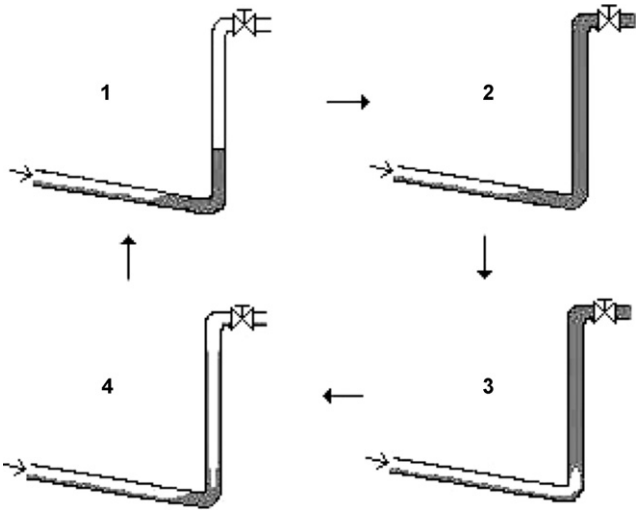

Fig. 3 – Illustration of the cyclic behavior (slug flow) in pipeline–riser systems.

liquid-filled riser. This is the type of slugs the small-scale lab rig described in this paper is built to recapture.

Under slug conditions a cyclic operation (limit cycle) is obtained. It is considered to consist of four steps (Schmidt et al., 1980; Taitel, 1986). These steps are illustrated in Fig. 3. Liquid accumulates in the low-point of the riser, blocking the gas (1). As more gas and liquid enters the system, the pressure will increase and the riser will be filled with liquid (2). After a while the amount of gas that is blocked will be large enough to blow the liquid out of the riser (3). After the blow-out, a new liquid slug will start to form in the low-point (4).

Terrain-induced slugs can become hundreds of meters long, whereas hydrodynamic slugs are relatively shorter. This is also the reason why terrain slugging is often referred to as severe slugging.

Slug flow has a negative impact on the receiving facilities during offshore oil and gas production due to the large fluctuations in flow rates and pressure. Frequent problems are unwanted flaring and reduced operating capacity. The fluctuating pressure also leads to a lot of strain on other parts of the system, such as valves and bends. The burden on the topside separators and compressors can in some cases become so large that it leads to damages and plant shutdown, representing huge costs for the producing company. Being able to remove slugging has a great economic potential and this is why lot of work and money has been spent on finding solutions to the problem.

It is possible to avoid or handle the slugs by changing the design of the system. Examples of this are: changing the pipeline topology, increasing the size of the separator, adding a slug catcher or installing gas lift. However, the implementation of this new equipment usually costs a lot of money.

Another option is changing the operating conditions by choking the topside valve. Also this comes with a drawback; the increased pressure in the pipeline leads to a reduced production rate and can lower the total recovery of the field that is being exploited.

In the last years there have been several studies on active control as a tool to "stabilize" the flow and thereby avoiding the slug flow regime. Mathematically, the objective is to stabilize a flow region which otherwise would be unstable. A simple analogue is stabilization of a bicycle which would be unstable without control. Schmidt et al. (1979) was the first to successfully apply an automatic control system on a

pipeline–riser system with a topside choke as actuator. Hedne and Linga (1990) showed that it was possible to control the flow using a PI controller and pressure sensors measuring the pressure difference over the riser. A similar controller was also implemented with success on the slug control rig described in this paper (Sivertsen and Skogestad, 2005). Lately different control strategies have also been implemented on production systems offshore with great success (Hollenberg et al., 1995; Courbot, 1996; Havre et al., 2000; Skofteland and Godhavn, 2003).

Active control changes the boundaries of the flow map presented in Fig. 2, so that it is possible to avoid the slug flow regime in an area where slug flow is predicted. This way it is possible to operate with the same average flow rates as before, but without the huge oscillations in flow rates and pressure. The advantages with using active control are large; it is much cheaper than implementing new equipment and it also removes the slug flow all together thereby removing the strain on the system. This way a lot of money can also be saved on maintenance. Also, it is possible to produce with larger flow rates than what would be possible by manually choking the topside valve.

Subsea measurements are usually included in the control structures that have been reported in the literature so far. Pressure measurements at the bottom of the riser or further upstream are examples of such measurements. When dealing with riser slugging, subsea measurements have proved to effectively stabilize the flow. When no subsea measurements are available, we will see that the task gets far more challenging.

Since subsea measurements are less reliable and much more costly to implement and maintain than measurements located topside, it is interesting to see if it is possible to control the flow using only topside measurements. Is it also possible to combine topside measurements in a way that improve the performance? And are the results comparable to the results obtained when using a controller based on subsea measurements?

Earlier studies on using only topside measurements are found in Godhavn et al. (2005) where experiments were performed on a larger rig and the flow was controlled using combinations of pressure and density measurements. This paper did not, however, compare the results found with what is obtainable using subsea measurements in the control structure. The present work compares experimental results using outlet (topside) measurements with results obtained using inlet ("subsea") measurements on a small-scale rig (Sivertsen and Skogestad, 2005). Similar experiments as the ones described in this paper were later performed on a *medium*-scale lab rig to investigate the effect the scale of the lab rig has on the quality of the controllers. These experiments are described in Sivertsen et al. (2008).

2. Case description

2.1. Experimental setup

To test different control configurations, a small-scale two-phase flow loop with a pipeline–riser arrangement was build at the Department of Chemical Engineering at NTNU, Trondheim (Baardsen, 2003). The flow consists of water and air, mixed together at the inlet of the system. Both the pipeline and the riser were made of a 20 mm diameter transparent rubber hose, which makes it easy to change the shape of the pipeline system. A schematic diagram of the test facilities is shown in Fig. 4.

From the inlet, which is the mixing point for the air and water, the flow is transported trough a 3 m long curved pipeline to the low-point at the bottom of the riser. Depending on different conditions such as water and air flow rates, slug flow may occur. At the top of the riser there is an acryl tank which serves as a separator, leading the water to a reservoir while the air is let out through an open hole in the top. The separator is thus holding atmospheric pressure.

From the reservoir the water is pumped back into the system through the mixing point using a Grundfos UPS 25-120 180 pump with a lifting capacity of 12 m. It is possible to adjust the power of the pump, thereby changing the pressure dependency of the inlet flow rate of the water. The pressure dependency during the experiments is discussed in Section 2.3, where periodic disturbances in the inlet flow rate of gas from the air supply system are also described.

For slugging to appear there must be enough air in the system to blow the water out of the 2.7 m long riser. This requires a certain amount of volume, which is accounted for by a 15 l acryl buffer tank (BT) between the air supply and the inlet. The volume of the gas can be changed by partially filling this tank with water.

The inlet flow rates of gas (Q_{air}) and water (Q_w) determine whether we will have slug flow in open-loop operation or not. The gas flow rate is measured at the inlet using a 2–10 l/min

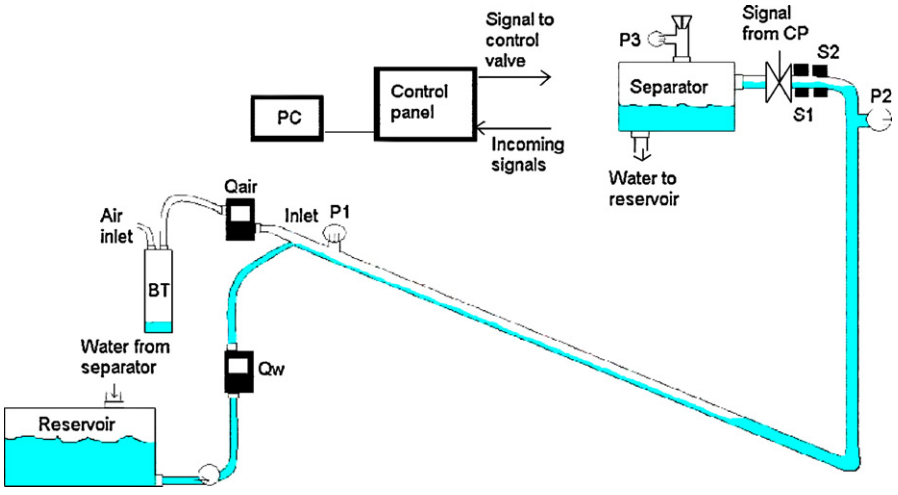

Fig. 4 – Experimental setup.

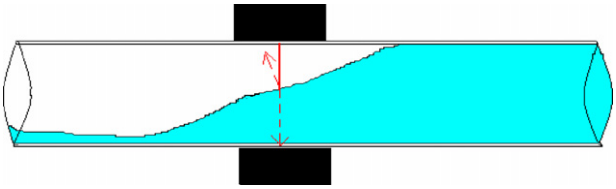

Fig. 5 – Reflection of light on water surface.

mass flow sensor from Cole–Parmer. The water flow rate was measured using a 2–60 l/min flow transmitter from Gemü. Typically inlet flow rates during an experiment are 5 l/min both for the gas and water.

Pressure sensors MPX5100DP from Motorola are located at the inlet (P_1) and topside (P_2). They measure the pressure difference between the atmospheric pressure and the pipeline pressure in the range 0–1 bar.

Typically average values for the pressure during the experiments are approximately 0.2 barg at the inlet and 0.05 barg just upstream the topside control valve.

Two fiber optic sensors (S_1, S_2) from Omron are placed just upstream the control valve in order to measure the water content in the pipeline. Water in the pipeline will attenuate the laser beam and weaken the signal send to the control panel. The measurements from the fiber optic slug sensors needed some filtering because of spikes caused by reflections of the laser beam on the water/air interface (Fig. 5). When correctly calibrated, the fiber optic sensors give a signal proportional to the amount of water the laser beam travels through in the pipeline and can be used to calculate the density ρ in the pipeline.

A pneumatic operated Gemü 554 angle seat globe valve with 20 mm inner diameter is installed at the top of the riser. A signal from the control panel sets the choke opening percentage of the valve. The valve responds well within a second to the incoming signal.

The control panel, consisting of Fieldpoint modules from National Instruments, converts the analog signals from the sensors into digital signals. The digital signals are then sent to a computer where they are continuously displayed and treated using Labview software. Depending on the control configuration, some of the measurements are used by the controller to set the choke opening for the control valve.

2.2. *Labview software*

Labview from National Instruments was chosen as the tool for acquiring, storing, displaying and analyzing the data from the different sensors. Also the valve opening of the topside valve was set from this program. The controllers was made using Labview PID controllers with features like integrator antiwindup and bumpless controller output for PID gain changes.

Also Labviews PID Control Input Filter has been used to filter the noisy fiber optic signals. This is a fifth-order low-pass FIR (Finite Impulse Response) filter and the filter cut-off frequency is designed to be 1/10 of the sample frequency of the input value.

2.3. *Disturbances*

Two of the largest sources of disturbances during the experiments were the variations in the air and water inlet flow rates. Experimental results with a valve opening of 10% and 100% (fully open) are shown in Fig. 2. When the valve is 10% open the flow is stable. However, there are 200 s fluctuations in the air inlet rate Q_a caused by the on–off controller used for the pressurized air facility at the laboratory. The fluctuations in water rate Q_w are however quite small for this valve opening.

When the topside valve is fully open the inlet pressure (P_1) starts to oscillate due to slug flow in the pipeline and large fluctuations in the water inlet flow were observed. The capacity of the water pump is pressure dependent, and oscillations in the inlet pressure cause the water rate to fluctuate between approximately 4.9 and 5.6 l/min as is seen from the lower right plot in Fig. 6. The pressure oscillations also lead to oscillations in the air inlet flow rate, which come in addition to the 200 s periodic fluctuations.

3. Controllability analysis and simulations

In order to have a starting point for the lab experiments, an analysis of the system has been performed. The analysis reveals some of the control limitations that can be expected using different measurements for control; see also Storkaas and Skogestad (2007) for a similar analysis of a simulation case study. Closed-loop simulations using these measurements are also described.

3.1. *Theoretical background*

Given the feedback control structure shown in Fig. 7 the measured output y is found by

$$y = G(s)u + G_d(s)d \tag{1}$$

Here u is the manipulated input, d is the disturbance to the system and n is measurement noise. G and G_d are the plant and disturbance models.

The location of RHP (Right Half Plane) poles and zeros in $G(s)$ impose bounds on the bandwidth of the system. These bounds can render it impossible to control the system when the RHP poles and -zeros are located close to each other. Skogestad and Postlethwaite (1996) show that a pair of pure complex RHP poles places a lower bound on the bandwidth of the closed-loop system:

$$w_c > 1.15|p| \tag{2}$$

whereas a real RHP-zeros imposes an *upper* bound

$$w_c < \frac{|z|}{2} \tag{3}$$

For an imaginary RHP-zero the bound is

$$w_c < 0.86|z| \tag{4}$$

When comparing Eq. (2) with (3) and (4) it is easy to see that if the RHP-zeros and -poles are located close to each other, bandwidth problems can occur. The closed-loop system also can be expressed as

$$y = Tr + SG_d d - Tn \tag{5}$$

where $T = (I + L) - 1L$, $S = (I + L) - 1$ and $L = GK$. L is the loop transfer function, whereas S is called the classical sensitivity function and gives the sensitivity reduction introduced by

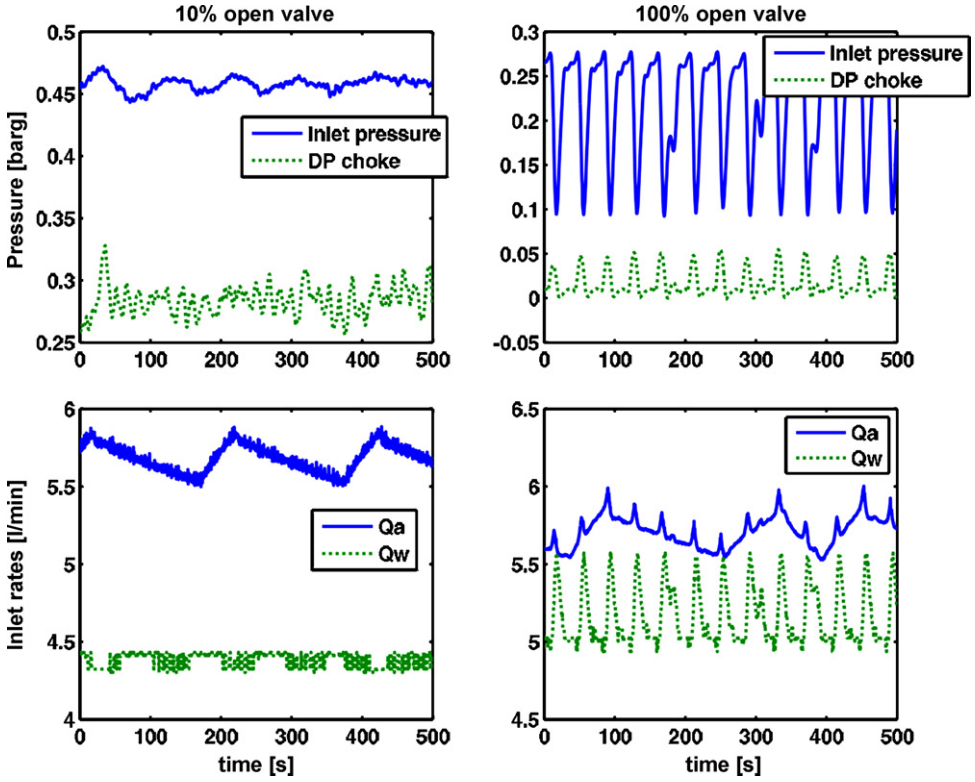

Fig. 6 – Experimental results without control. Top: Inlet and outlet pressures. Bottom: Disturbances in the inlet water flow rate (Q_w) and air inlet rate (Q_a).

the feedback loop. The input signal is

$$u = KSr - KSG_d d - KSn \tag{6}$$

and the control error $e = y - r$ is

$$e = -Sr + SG_d d - Tn \tag{7}$$

From Eqs. (5) to (7) it is obvious that the magnitude for transfer functions S, T, SG, KS, KSG_d and SG_d give valuable information about the effect u, d and n have on the system. In order to keep the input usage u and control error e small, these closed-loop transfer functions also need to be small. There are however some limitations on how small the peak values of these transfer functions can be. The locations of the RHP-zeros and -poles influence these bounds significantly.

3.1.1. *Minimum peaks on S and T*

Skogestad and Postlethwaite (1996) shows that for each RHP-zero z of G(s) the sensitivity function must satisfy Eq. (8) for closed-loop stability.

$$||S||_\infty \geq \prod_{i=1}^{Np} \frac{|z + p_i|}{|z - p_i|} \tag{8}$$

Here $||S||_\infty$ denotes the maximum frequency response of S. This bound is tight for the case with a single RHP-zero and no time delay. Chen (2000) shows that the same bound is tight for T.

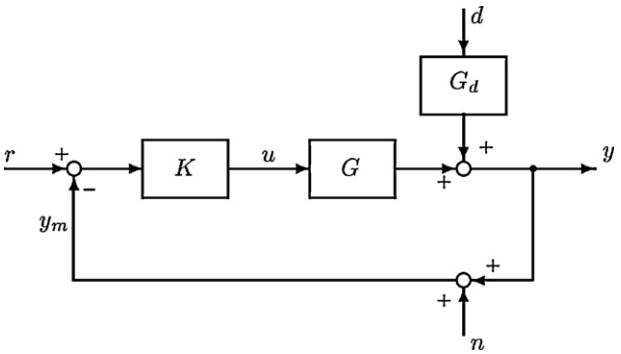

Fig. 7 – One degree-of-freedom negative feedback control structure (Skogestad and Postlethwaite, 1996).

3.1.2. *Minimum peaks on SG and SG_d*

The transfer function SG is required to be small for robustness against pole uncertainty. Similar, SG_d needs to be small in order to reduce the effect of the input disturbances on the control error signal e. In Skogestad and Postlethwaite (1996) the following bounds are found for SG and SG_d

$$||SG||_\infty \geq |G_{ms}(z)| \prod_{i=1}^{Np} \frac{|z + p_i|}{|z - p_i|} \tag{9}$$

$$||SG_d||_\infty \geq |G_{d,ms}(z)| \prod_{i=1}^{Np} \frac{|z + p_i|}{|z - p_i|} \tag{10}$$

These bounds are valid for each RHP-zero of the system. Here G_{ms} and $G_{d,ms}$ are the "minimum, stable version" of G and G_d with RHP poles and zeros mirrored into the LHP.

3.1.3. *Minimum peaks on KS and KSG_d*

The peak on the transfer function KS needs to be small to avoid large input signals in response to noise and disturbances, which could result in saturation. Havre and Skogestad (2002)

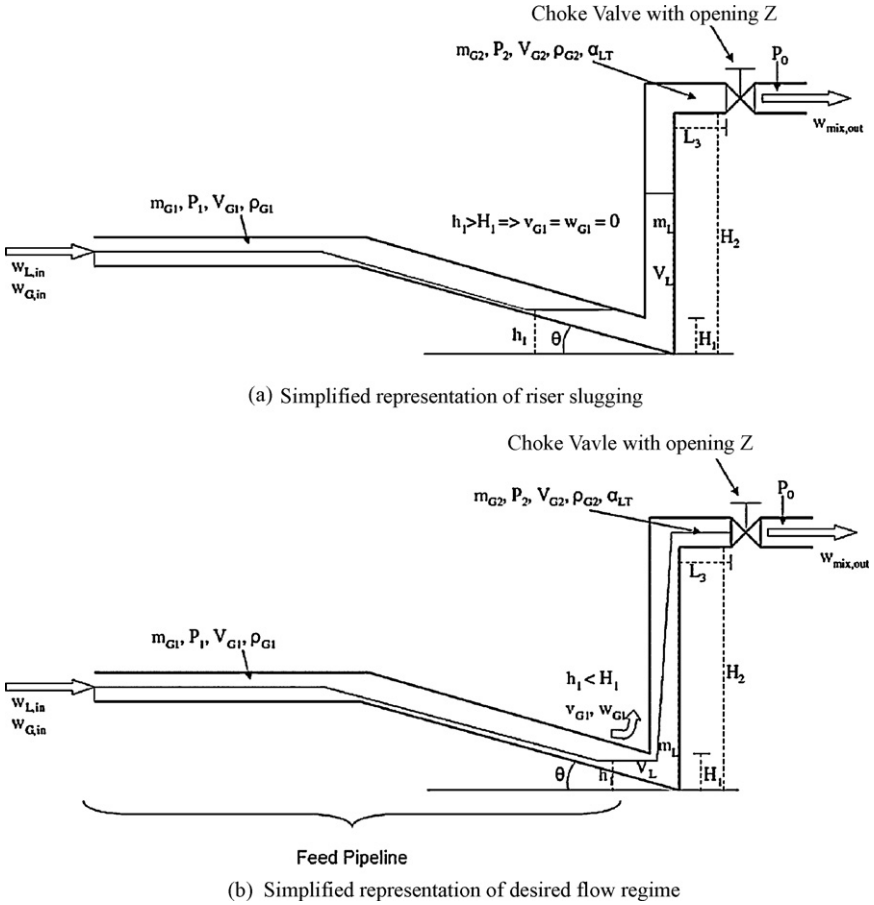

Fig. 8 – Storkaas' pipeline–riser slug model (Storkaas et al., 2003).

derives the following bound on KS

$$||KS||_\infty \geq |G_s^{-1}(p)| \tag{11}$$

which is tight for plants with a single real RHP-pole p. Havre and Skogestad (2002) also finds

$$||KSG_d||_\infty \geq |G_s^{-1}(p)G_{d,ms}(p)| \tag{12}$$

When analyzing a plant, all of the closed-loop transfer functions should be considered.

3.2. *Modeling*

Storkaas et al. (2003) have developed a simplified model to describe the behavior of pipeline–riser slugging. One of the advantages of the model is that it is well suited for controller design and analysis. It consists of three states; the holdup of gas in the feed section (m_{G1}), the holdup of gas in the riser (m_{G2}), and the holdup of liquid (m_L). The model is illustrated by Fig. 8 and is very simplified. The main justification for its use is that it matches very well the actual data; at least for the purposes of feedback control. This is further discussed by Storkaas and Skogestad (2007), who compared the control properties of simple three-state model with a more detailed two-fluid model.

Using this model we are able to predict the variation of system properties such as pressures, densities and phase fractions and analyze the system around desired operation points. After entering the geometrical and flow data for the lab rig, the model was tuned as described in Storkaas et al. (2003) to fit the open-loop behavior of the lab rig. The model and tuning procedure is further described in Appendix A. Model data and tuning parameters for the small-scale lab rig are presented in Table 1.

A bifurcation diagram of the system is plotted in Fig. 9. It was found by open-loop simulations (without control) at dif-

Table 1 – Model data parameters.

Parameter	Symbol	Value
Inlet flow rate gas [kg/s]	$w_{G,in}$	$1.145e-4$
Inlet flow rate water [kg/s]	$w_{L,in}$	0.090
Valve opening at bifurcation point	z	0.16
Inlet pressure at bifurcation point [barg]	$P_{1,stasj}$	0.28
Topside pressure at bifurcation point [barg]	$P_{2,stasj}$	0.125
Separator pressure [barg]	P_0	0
Liquid level upstream low-point at bifurcation point [m]	$h_{1,stasj}$	$9.75e-3$
Upstream gas volume [m^3]	V_{G1}	$6.1e-3$
Feed pipe inclination [rad]	θ	1e3
Riser height [m]	H_2	2.7
Length of horizontal top section [m]	L_3	0.2
Pipe radius [m]	r	0.01
Exponent in friction expression	n	16
Choke valve constant [m^{-2}]	K_1	$2.23e-4$
Internal gas flow constant	K_2	0.193
Friction parameter [s^2/m^2]	K_3	3.4e3

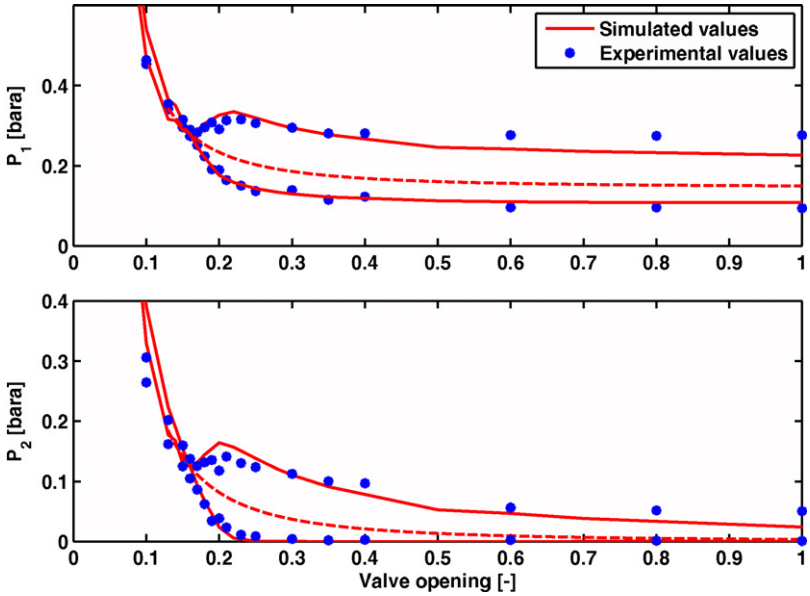

Fig. 9 – Bifurcation plots showing the open-loop behavior of the system.

ferent valve openings and gives information about the valve opening for which the system goes unstable. Also the amplitude of the pressure oscillations for the inlet and topside pressure (P_1 and P_2) at each valve opening can be seen from the plot.

The upper line in the bifurcation plots shows the maximum pressure at a particular valve opening and the lower line shows the minimum pressure. The two lines meet at around 16% valve opening. This is the largest valve opening which gives stable operation when no control is applied for this particular system. When Storkaas' model is properly tuned, the bifurcation point from the model will match the one from the experimental data. From the bifurcation diagram in Fig. 9 it is seen that the tuned model values fit the results from the lab quite well. The dashed line in the middle shows the unstable steady-state solution. This is the desired operating line with closed-loop operation.

Fig. 10 shows some of the simulations performed in order to find the bifurcation diagram. The plots show that the frequency predicted by the model is approximately 50% higher than the frequency of the slugs in the lab. There exist other models that better predict the slug flow region. However, the main purpose of our simple model is to use it for control. Thus, the most important factor is that the model gives an acceptable description of the desired non-slug regime, which is unstable without control (the middle dashed curve in Fig. 9). The fact that the model gives a reasonable description of the undesired slug flow regime (Fig. 10) may be viewed upon as a bonus. A simple analogy is the following: if we want to use control to stabilize a bicycle then we need a good model for the bicycle in its desired position ("non-slug regime") and not a model of how it behaves when lying on the ground ("slug flow regime").

In Fig. 11 a root-locus diagram of the system is plotted. This plot shows how the poles cross into the RHP as the valve opening reaches 16% from below. This also confirms the results plotted in the bifurcation diagram in Fig. 9.

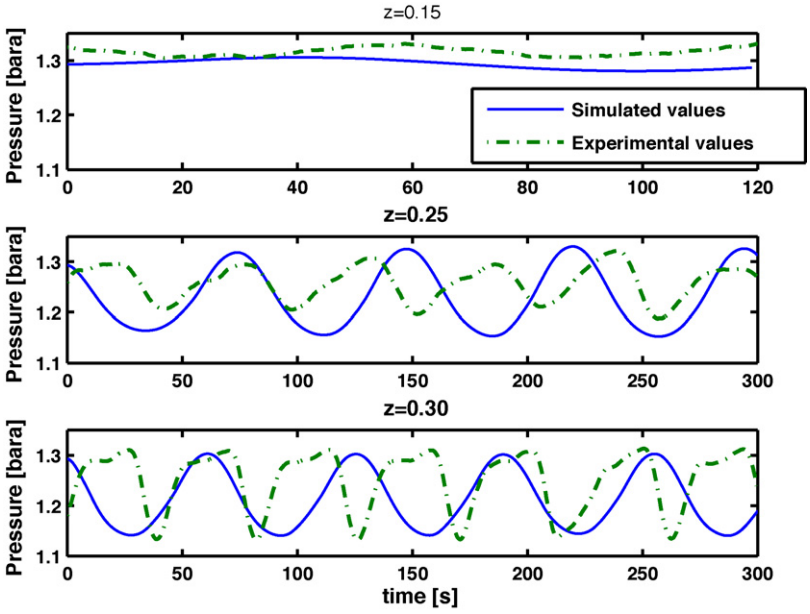

Fig. 10 – Open-loop behavior of inlet pressure P_1 for valve openings 15, 25 and 30%.

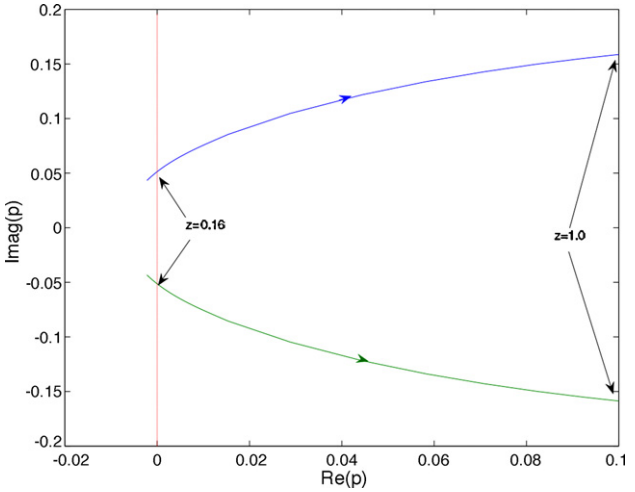

Fig. 11 – Root-locus plot showing the trajectories of the RHP open-loop poles when the valve opening varies from 0 (closed) to 1 (fully open).

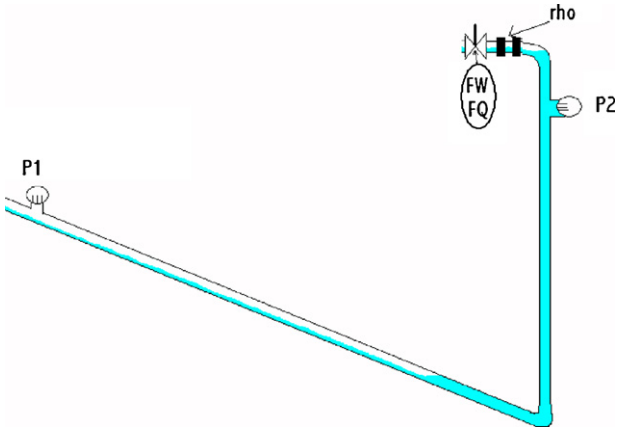

Fig. 12 – Measurement candidates for control.

3.3. *Analysis*

The model can now be used to explore different measurement alternatives for controlling the flow. The lab rig has four sensors as described in Section 2. There are two pressure sensors; one located at the inlet (P_1) and one located topside upstream the control valve (P_2). Also two fiber optic water holdup measurements are located upstream the control valve. Using these measurements it is possible to estimate the density (ρ) and flow rates (F_Q, F_W) through the control valve. Fig. 12 shows the five different measurement candidates (y). The control input (u) is the valve opening.

In Section 3.1 it was shown how the locations of the RHP poles and zeros had a big influence on the controllability of the system. By scaling the system and calculating the sensitivity peaks it is possible to get a picture of how well a controller, using one of these measurements, can perform.

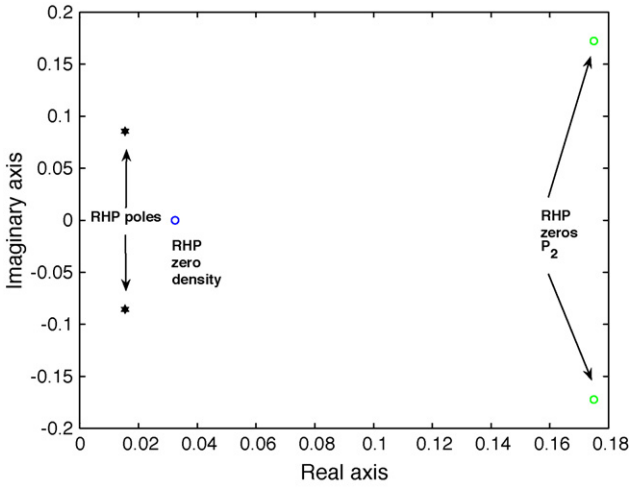

Fig. 13 – Plot-zero map for valve opening 30%.

The process model G and disturbance model G_d were found from a linearization of Storkaas' model around two operation points. The model was then scaled as described in Skogestad and Postlethwaite (1996). The process variables were scaled with respect to the largest allowed control error and the disturbances were scaled with the largest variations in the inlet flow rates in the lab. The disturbances were assumed to be frequency independent. The input was scaled with the maximum allowed positive deviation in valve opening since the process gain is smaller for large valve openings. For measurements $y = [P_1; P_2; \rho; F_W; F_Q]$ the scaling matrix is $De = diag[0.1\ 0.05\ 100\ 0.01\ 1e^{-5}\ 0.1]$. The scaling matrix for the disturbances is $Dd = diag\ [1e^{-5}\ 1e^{-2}]$. This represents approximately 10% change in the inlet flow rates from the nominal values of $1.145e^{-4}$ kg/s (5.73 l/min) for gas and $90e^{-3}$ kg/s (5.4 l/min) for water. The input is scaled $Du = 1 - z_{nom}$ where z_{nom} is the nominal valve opening.

Tables 2 and 3 presents the controllability results. The location of the RHP poles and zeros are presented for valve openings 25 and 30%, as well as stationary gain and lower bounds on the closed-loop transfer functions described in Section 3.1. The only two measurements of the ones considered in this paper which introduces RHP-zeros into the system, are the topside density ρ and pressure P_2. The pole location is independent of the input and output (measurement), but the zeros may move. From the bifurcation plot in Fig. 9 it is seen that both of these valve openings are inside the unstable area. This can also be seen from the RHP location of the poles.

In Fig. 13 the RHP poles and relevant RHP-zeros are plotted together. The RHP-zeros are in both cases located quite close to the RHP poles, which results in the high peaks especially

Table 2 – Control limitation data for valve opening 25%. Unstable poles at $p = 0.010 \pm 0.075i$.

Measurement	RHP-zeros	Stationary gain	Minimum bounds				
		$\lvert G(0)\rvert$	$\lvert S\rvert$	$\lvert SG\rvert$	$\lvert KS\rvert$	$\lvert SG_d\rvert$	$\lvert KSG_d\rvert$
P_1 [bar]	–	3.20	1.00	0.00	0.14	0.00	0.055
P_2 [bar]	$0.18 \pm 0.17i$	5.97	1.13	1.59	0.091	0.085	0.055
ρ [kg/s]	0.032	0.70	1.20	4.62	0.048	0.31	0.056
F_W [kg/s]	–	0.00	1.00	0.00	0.015	1.00	0.055
F_Q [m^3/s]	–	2.59	1.00	0.00	0.015	0.00	0.055

Table 3 – Control limitation data for valve opening 30%. Unstable poles at $p = 0.015 \pm 0.086i$.

Measurement	RHP-zeros	Stationary gain	Minimum bounds				
		$\lvert G(0)\rvert$	$\lvert S\rvert$	$\lvert SG\rvert$	$\lvert KS\rvert$	$\lvert SG_d\rvert$	$\lvert KSG_d\rvert$
P_1 [bar]	–	1.85	1.00	0.00	0.34	0.00	0.086
P_2 [bar]	$0.18 \pm 0.17i$	3.44	1.22	1.25	0.23	0.085	0.079
ρ [kg/s]	0.032	0.41	1.26	2.86	0.091	0.31	0.081
F_W [kg/s]	–	0.00	1.00	0.00	0.028	1.00	0.079
F_Q [m^3/s]	–	1.53	1.00	0.00	0.028	0.00	0.079

for sensitivity function SG but also for S. From this we can expect problems when trying to stabilize the flow using these measurements as single measurements.

The stationary (steady-state) gain found when using the volumetric flow rate F_W is approximately zero, which can cause a lot of problems with steady-state control of the system. Also the stationary gain for the plant using density ρ as measurement has a low stationary gain. The model is however based on constant inlet flow rates. The stationary gain for F_W predicted by the model is 0, which means that it is not possible to control the steady-state behavior of the system and the system will drift. Usually the inlet rates are pressure dependent, and the zeros for measurements F_Q and F_W would be expected to be located further away from the origin than indicated by Tables 2 and 3.

When comparing $|KS|$ and $|KSG_d|$ from the two tables, it is obvious that the peak values for these transfer functions increase with valve opening for all the measurement candidates, indicating that controlling around an operating point with a larger valve opening increases the effect disturbances and noise have on the input usage.

Figs. 14 and 15 show the Bode plots for the different plant models and disturbance models respectively. The models were found from a linearization of the model around valve opening 25%. For the volumetric flow rate measurement, F_W, the value of the disturbance model G_dW is higher than plant model GW for low frequencies. For acceptable control we require $|G(jw)| > |G_d(jw)| - 1$ for frequencies where $|G_d| > 1$ (Skogestad and Postlethwaite (1996)). In this case, both $|G_dW|$ and $|GW|$ are close to zero, which means problems can occur for this measurement.

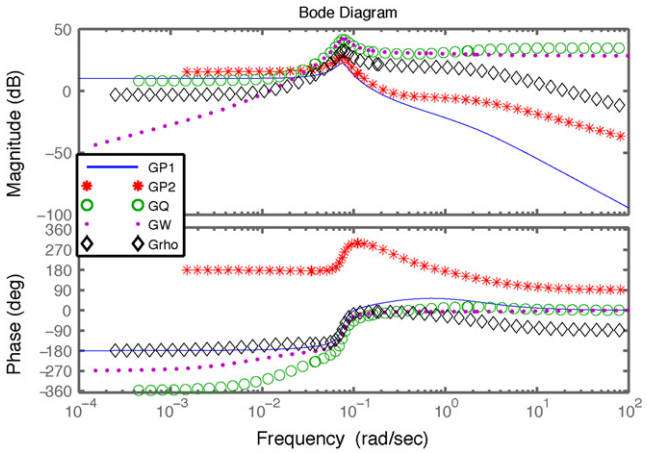

Fig. 14 – Bode plots for plant models G using different measurements.

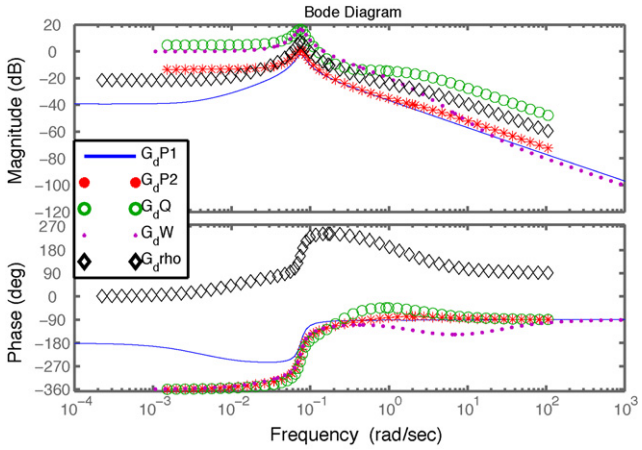

Fig. 15 – Bode plots of disturbance models G_d using different measurements.

3.4. *Simulations*

Closed-loop simulations using Stokaas' model were performed using alternative measurements (y) in a feedback loop with a PI controller. Fig. 16 shows this control structure using the inlet pressure P_1 as the measurement.

Fig. 17 compares the simulated results using four different measurement candidates. Disturbances in the inlet flow rates for the gas and water, as described in Section 2.3, are also included in these simulations. The only measurement that is not included is the topside pressure P_2, as the corresponding controller was not able to stabilize the flow.

At first, the controller is turned off and the system is left open-loop with a valve opening of 20% for approximately 5–10 min. From the bifurcation diagram in Fig. 9 it was shown that the system goes unstable for valve openings larger than

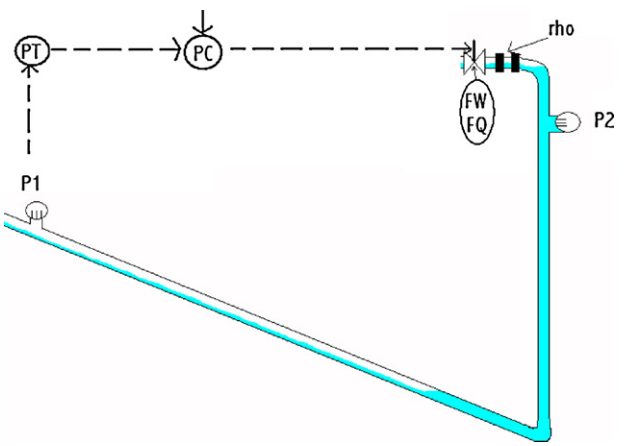

Fig. 16 – Feedback control using PI controller with inlet pressure P_1 as measurement.

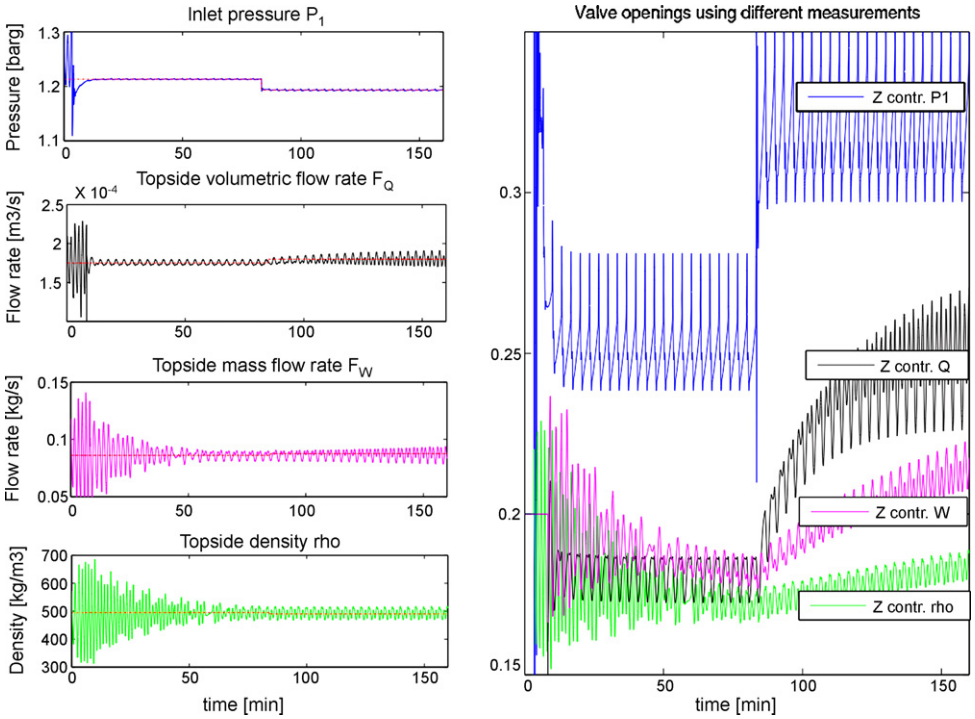

Fig. 17 – Simulated results when using PI controllers to stabilize the flow with different choice of measurements.

16%. As expected, the pressure and flow rates start to oscillate due to the effects of slug flow.

When the controller is activated, the control valve starts working as seen from the right plot in Fig. 17. The aim of the simulation study is to see how far into the unstable region it is possible to control the flow with satisfactory performance. A larger valve opening gives higher production with a given pressure-dependent source.

As expected the measurement giving the best result was inlet pressure P_1. The upper left plot shows how the controller quickly stabilizes at the desired set point. The average valve opening is 25%, which is far into the unstable region. After about 70 min the set point for the pressure is decreased, and the valve opening is now larger than 30%. Still the performance of the controller is good.

The figure also shows the results using a topside volumetric flow rate F_Q, mass flow rate F_W and the density ρ. Not surprisingly, the density measurement was not very well suited, as was expected from the analysis in Section 3.3. It was possible to control the flow using this measurement, but not at an average valve opening larger than 17–18% which is just inside the unstable area. The benefits of using control are therefore negligible.

The relatively small oscillations seen in each plot have a period of 200 s (3.3 min). They are caused by the periodic oscillations of the inlet air flow rate. The results using the topside pressure P_2 are not included in the figure. This is because it was not possible to stabilize the flow inside the unstable region using this measurement. Although the analysis suggested otherwise, the disturbances added in the simulations might have had a larger effect on this measurement than on the others.

Sometimes control configurations using *combinations* of measurements can improve the performance when compared with controllers using single measurements. This is why cascade controllers using different combinations of the topside measurements have been applied to the system. Fig. 18 shows

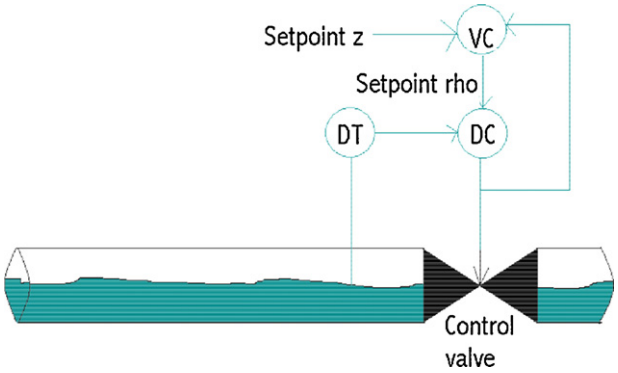

Fig. 18 – Cascade controller using topside measurements of density ρ and valve opening z.

an example of such a control configuration. The inner loop controls the topside density ρ, while the set point for this inner controller is set by an outer loop controlling the valve opening. This way drift due to the low stationary gain for ρ is avoided.

The results from simulations using this control structure are plotted in Fig. 19. The set point for the outer loop controller, controlling the valve opening, is increased from 17% to 18% after approximately 170 min. The flow then quickly becomes unstable, even though the valve opening is just inside the unstable region. Thus, the results using this controller are approximately the same as when using the PI controller with density ρ.

Using one of the other measurements, F_Q, F_w or P_1 in the inner loop instead would probably give better results as these measurement stabilize the flow better than the density measurement ρ.

4. Experimental results

The results from the analysis and simulations using the model suggest that of the topside measurements, the best is the vol-

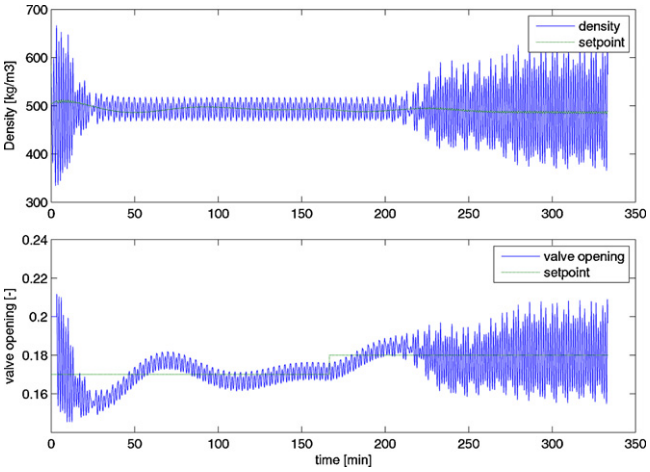

Fig. 19 – Simulation results using density ρ and valve opening z as measured variables in a cascade control structure.

umetric or mass flow rates F_Q, followed by the mass flow rate F_W and the topside density. In the simulations it was not possible to stabilize the flow using the topside pressure (p_1). The objective is now to study this experimentally.

An attempt was made to control the flow and avoid slugging using the fiber optic signal as measurement in the inner loop of the control structure shown in Fig. 18. The fiber optic signal can be compared with a scaled version of a density measurement, as the large density differences between liquid and vapour is essentially the same as the liquid volume fraction in the pipe, recorded by the fiber optic sensors. Flow measurements are not included in the experiments because no direct measurements were available. One alternative would be to calculate the flow using a valve equation for two-phase flow and the topside pressure measurement P_2, fiber optic signals S_1 and S_2 and the valve opening z. However, two-phase flow valve equations are empirical and also quite complicated, and it seemed easier first to use the measurements at hand.

In the experiments three different combinations of measurements were tested in a cascade control structure similar to the on shown in Fig. 18 in Section 3. In case (a), inlet pressure P_1 is used in the inner loop and the valve opening z in the outer loop. Even though P_1 is not a topside measurement, the results using this controller serve as a basis to compare the other two controllers with. The other two control structures use the fiber optic signal in the inner loop, and had either (b) the valve opening z (Fig. 18) or (c) the topside pressure P_2 as a measurement in the outer loop.

The experimental results in Fig. 20 show that stabilizing control was achieved for all three cases. First the system was left open-loop with a valve opening of 25%. Since this is well inside the unstable slug-flow region, the pressures and density in the system is oscillating. After about 100 s the controllers are turned on, and in all three cases the controllers are able to stabilize the flow. When the controllers are turned off after 500–600 s, the flow quickly becomes unstable again. The thick lines indicated the set points for the different controllers. In plots (a) and (b) in Fig. 20 the valve opening set point for the outer loop was 25% fully open, whereas for the experiment presented in plot (c) the set point for the topside pressure P_2 in the outer loop was 0.056. Earlier experiments had shown that this lead to an average valve opening of about 25%.

From the analysis and simulations presented in Section 3, it is expected that the control structure with the inlet pressure P_1 in the inner loop would perform best. Also, the fiber optic measurement is very noisy as the plots in Fig. 20 show. Despite all this, looking at the experimental results the differences are less obvious. In fact, using the fiber optic signal as the inner

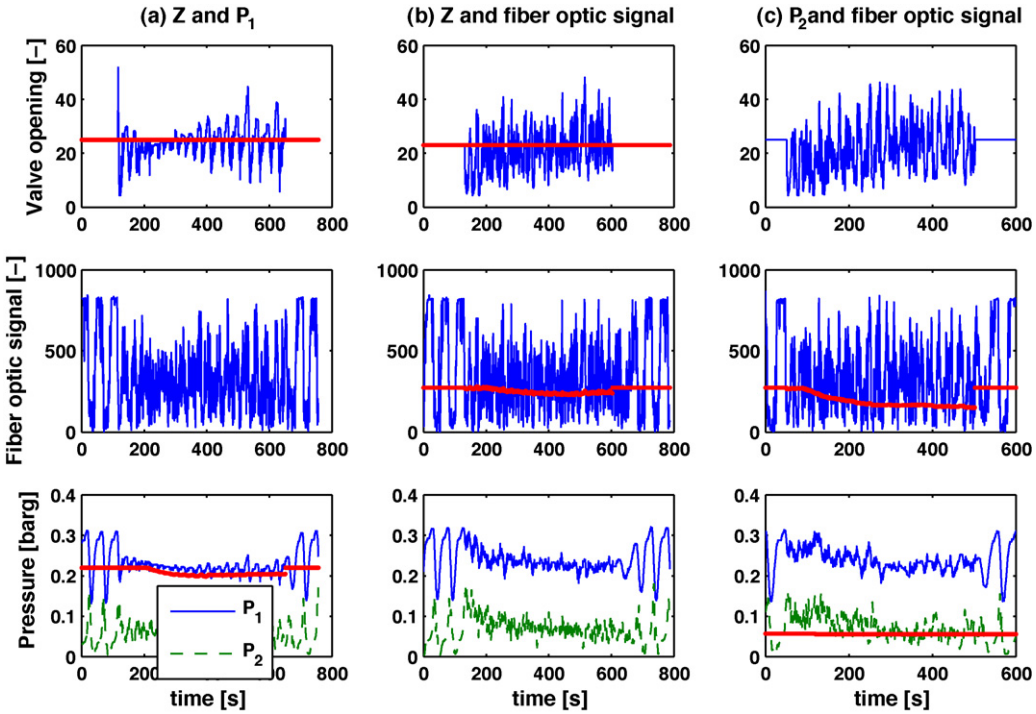

Fig. 20 – Experimental cascade control experiments at valve opening of approximately 25% using three control structures; (a) P_1 (inner loop) and z (outer loop), (b) fiber optic signal (inner loop) and z (outer loop), (c) fiber optic signal (inner loop) and P_2 (outer loop).

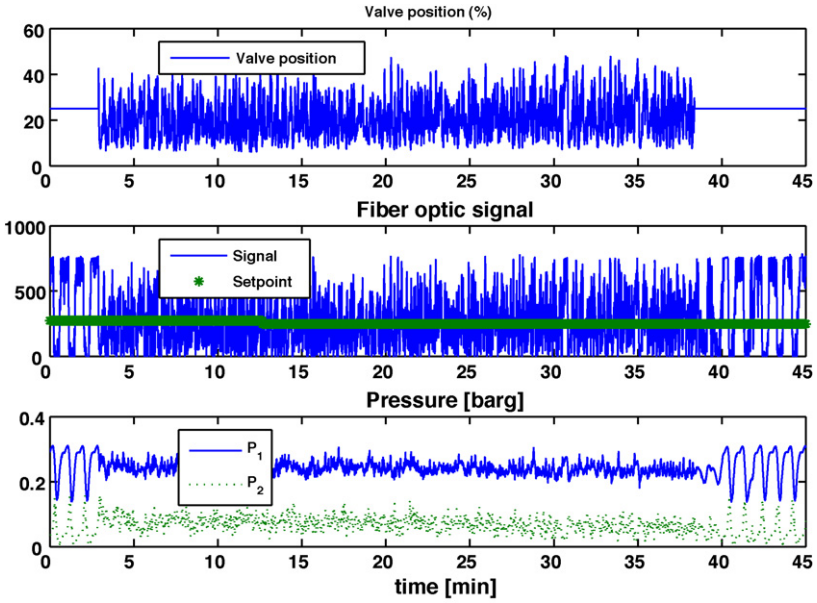

Fig. 21 – Experimental results using a PI controller with fiber optic ψ signal as the single measurement (no outer loop added).

measurement works quite well, contradicting the results from the analysis in Section 3.

The main reason for adding the outer loop is to avoid drift in the inner loop caused by the low steady-state gain shown in Tables 2 and 3. Since the results from the experiments using a cascade configuration by far outperform the results from the simulations, it was reason to question the values given by the model. This is why an attempt was made to see whether it was possible to control the flow using the fiber optic signal as *only* measurement for control. Fig. 21 shows the results using a PI controller and the fiber optic signal.

Also now the controller manages to stabilize the flow. The system does not seem to drift, which means that the steady-state gain is not too small. Controlling the flow at a larger average valve opening led to reduced performance and the flow either became unstable or the controller did not manage to satisfactory keep the measurements at the desired set points (large fluctuations).

In general, as the analysis showed, the control task gets harder as the valve opening increases. This is due to the fact that the gain is reduced as the valve opening gets larger. By gradually increasing the average valve opening, either by increasing the set point for valve opening in the outer loop or, for case (c), reducing the set point for the density, the effect of this increase in valve opening was found.

Some results are plotted in Appendix B for the three cascade structures (a), (b) and (c) in Fig. 21. Here it is seen that the effect of increasing the average valve opening from approximately 24% to 32% using P_1 as measurement leads to increasingly larger fluctuations around the set points. The same experiments were performed using the fiber optic signal as measurement in the inner loop with (b) z and (c) P_2 in the outer loop. As expected, the system goes unstable as the valve opening is increased. The average valve opening for which the system goes unstable using these controllers were approximately (b) 26% and (c) 29%. This is however far into the unstable region. Operating at these valve openings instead of 15% with stable flow *without* control will in most cases lead to a significantly higher production and recovery rate for a given well or reservoir.

5. Discussion

When comparing different controllers, the tuning of the controllers has a large influence on the results. None of the controllers described in this paper have been fine-tuned and the results might be improved further with some more work. This is why the maximum average valve opening for which the controllers stabilize the flow, presented in Section 4, might be increased with better tuning. However, from the results it seems obvious that all three controllers perform well up to approximately 25% valve opening and that as the valve opening moves towards an average value of 30% the controller performance decreases for all the controllers.

The timing for when the controller was activated seemed to have an effect in how quickly the controller managed to control the flow. Activating the controller at a pressure peak in the system was most advantageous.

It is important to note that the model used for the analysis is very simplified. It was used as a tool to see which problems might occur in the lab, and find the underlying reasons for the problems. When comparing the experimental results with analysis and simulations using Storkaas' model prior to the experiments, it was found that the experimental results were far better than the model predicted when using the fiber optic signal as a density measurement. On the other hand, the topside pressure P_2 could not be used for stabilization, in agreement with Storkaas' model.

An attempt was made to model the small-scale rig using the multiphase simulator OLGA from Scandpower Petroleum Technologies. However, the simulations seemed to fail due to numerical errors, which could be caused by the small-scale nature of the rig.

Even though results using only a PI controller and a single topside density measurement seemed to work very well, without the expected steady-state drift, there are other advantages in adding an outer loop.

One example of such is that it may be more intuitive to understand what is going on with the plant when adjusting the set point for the valve opening rather than the set point for the topside density or flow rates.

The experiments have been conducted on a small-scale rig with only 20 mm inner diameter pipeline. Whether or not the results can be directly applied to larger test facilities was further investigated in Sivertsen et al. (2008). The results from these experiments showed that similar control schemes as the ones described in this paper, also were successful when applied to a medium scale lab rig with a 10 m high riser and 7.6 cm diameter pipelines.

6. Conclusion

This paper presents results from a small-scale riser laboratory rig where the aim was to control the flow using only topside measurements and thereby avoiding slug flow in the pipeline.

The results were good in the sense that it was possible to control the flow with good performance far into the unstable slug-flow region. In order to avoid the slug merely by choking the topside valve it would be necessary to operate with a valve opening of 15%, whereas here it was shown that it was possible to control the flow with an average valve opening of 25%, despite very noisy measurements. This makes it possible to produce with a larger production rate and increase the total recovery from the producing oil field.

Acknowledgments

The authors would like thank former students who have been involved in the project and helped in building the lab rig; Ingvald Baardsen and Morten Søndrol. Also the staff at the Faculty of Natural Sciences and Technology has been great in helping with equipment and software problems. We would also like to thank StatoilHydro and the Norwegian Research Council for their financial support.

Appendix A. Storkaas' model

The main assumptions are:

A1.	Neglected liquid dynamics in the upstream feed pipeline, that is, constant liquid velocity in this section.
A2.	Constant gas volume V_{G1} (but possible varying mass of gas) in the feed pipeline. This follows from assumption A1 if we also neglect the liquid volume variations due to variations in the liquid level h_1 at the low-point.
A3.	Only one dynamical state (m_L) for liquid holdup in the riser section. This state includes both the liquid in the riser and in the low-point section (with level h_1)
A4.	Two dynamical states for gas holdup (m_{G1} and m_{G2}), occupying the volumes V_{G1} and V_{G2}, respectively. The gas volumes are "connected" by a pressure-flow relationship in the low-point.
A5.	Ideal gas behavior.
A6.	Stationary pressure balance over the riser (between pressures P_1 and P_2).
A7.	Simplified valve equation for gas and liquid mixture leaving the system at the top of the riser.
A8.	Constant temperature.

A.1. Model fundamentals

The model has three dynamical states, as stated by assumptions A3 and A4:

- mass of liquid m_L in the riser and around the low-point
- mass of gas m_{G1} in the feed section
- mass of gas m_{G2} in the riser

The corresponding mass conservation equations are

$$\frac{dm_L}{dt} = w_{L,in} - w_{L,out} \tag{A.1}$$

$$\frac{dm_{G1}}{dt} = w_{G,in} - w_{G1} \tag{A.2}$$

$$\frac{dm_{G2}}{dt} = w_{G1} - w_{G,out} \tag{A.3}$$

Computation of most of the system properties such as pressures, densities and phase fractions are then straightforward.

Some comments:

- The stationary pressure balance over the riser A6 is assumed to be given by

$$P_1 - P_2 = \bar{\rho} g H_2 - \rho_L g h_1 \tag{A.4}$$

  Here, $\bar{\rho}$ is the average mixture density in the riser. The use of a stationary pressure balance is justified because the pressure dynamics are significantly faster than the time scales in the control problem. For long pipelines, it might be necessary to add some dynamics (i.e. time delay) between the pipeline pressure P_1 and the measured pressure if the pressure sensor is located far from the riser.
- The boundary condition at the inlet (inflow $w_{G,in}$ and $w_{L,in}$) can either be constant or pressure dependent. A simplified valve equation for incompressible flow is used to describe the flow through the choke valve,

$$w_{mix,out} = K_1 z \sqrt{\rho_T (P_2 - P_0)} \tag{A.5}$$

- The most critical part of the model is the phase distribution and phase velocities in the riser. The gas velocity is based on an assumption of purely frictional pressure drop over the low-point and the phase distribution is based on an entrainment model. This is discussed in more detail below.

Relationship between gas flow into riser and pressure drop

When the liquid is blocking the low-point ($h_1 > H_1$), the gas flow w_{G1} is zero.

$$w_{G1} = 0, h_1 \geq H_1 \tag{A.6}$$

When the liquid is not blocking the low-point ($h_1 < H_1$), the gas will flow from V_{G1} to V_{G2} with a mass rate w_{G1}[kg/s]. From physical insight, the two most important parameters determining the gas rate are the pressure drop over the low-point and the free area given by the relative liquid level ($(H_1 - h_1)/H_1$) at the low-point. This suggests that the gas transport could be described by a valve equation, where the pressure drop is driving the gas through a "valve" with opening $(H_1 - h_1)/H_1$. Based on trial and error, we propose to use the following "valve

equation":

$$w_{G1} = K_2 f(h_1)\sqrt{\rho_{G1}(P_1 - P_2 - \rho_L g \alpha_L H_2)} \tag{A.7}$$

where $f(h_1) = \hat{A}(H_1 - h_1)/H_1$ and $\hat{A}$ is the gas flow cross-section at the low-point. Note that $f(h_1) = \hat{A}(H_1 - h_1)/H_1$ is approximately quadratic in the "opening" $(H_1 - h_1)/H_1$.

Separating out the gas velocity with $w_{G1} = v_{G1}\rho_{G1}\hat{A}$ yields

$$v_{G1} = \begin{cases} K_2 \dfrac{H_1 - h_1}{H_1}\sqrt{\dfrac{P_1 - P_2 - \rho_L g \alpha_L H_2}{\rho_{G1}}} & h_1 < H_1 \\ 0 & h_1 \geq H_1 \end{cases} \tag{A.8}$$

A.2. Entrainment equation

The final important element of the model is the fluid distribution in the riser. This distribution can be represented in several ways. One approach is to use a slip relation to relate the liquid velocity to the gas velocity and use the velocities to compute the distribution. This is similar to the approach used in a drift flux model (Zuber and Findlay, 1965). We made several attempts to derive a model based on this approach, but were not successful.

Another approach is to model directly the volume fraction of liquid (α_{LT}) in the stream exiting the riser. We found that this approach was better suited for our purposes. The liquid fraction will lie between two extremes:

1. When the liquid blocks the flow such that there is no gas flowing through the riser ($v_{G1} = 0$), we have $\alpha_{LT} = \alpha^*_{LT}$. In most cases we will then have only gas exiting the riser and $\alpha^*_{LT} = 0$. However, eventually the entering liquid may cause the liquid to fill up the riser and α^*_{LT} will exceed zero.
2. When the gas velocity is very high there will be no slip between the phases, $\alpha_{LT} = \alpha_L$, where α_L is average liquid fraction in the riser.

The transition between these two extremes should be smooth. We assume that the transition depends on a parameter q and represented by the entrainment equation

$$\alpha_{LT} = \alpha^*_{LT} + \frac{q^n}{1 + q^n}(\alpha_L - \alpha^*_{LT}) \tag{A.9}$$

The parameter n is used to tune the slope of the transition.

The final parameter q in (A.9) must depend on the gas velocity in the system. To derive this relationship, we note that the entrainment of liquid by the gas in the riser is somewhat similar to flooding in gas–liquid contacting devices such as distillation columns. The flooding velocity is equal to the terminal velocity for a falling liquid drop and is given by

$$v_f = k_f\sqrt{\frac{(\rho_L - \rho_G)}{\rho_G}} \tag{A.10}$$

This expression only gives a yes/no answer to whether it is flooding ($v_G > v_f$) or not ($v_G < v_f$). To get a smooth transition, we use the square of the ratio of the internal gas velocity v_{G1} to the flooding velocity v_f. Thus, $q = k(v_{G1}/v_f)^2$ and introducing v_f from (A.10) gives

$$q = \frac{K_3 \rho_{G1} v^2_{G1}}{\rho_L - \rho_{G1}} \tag{A.11}$$

where $K_3 = k/k_f^2$. Eq. (A.11) combined with (A.9) produces the transition. The tuning parameter K_3 will shift the transition along the horizontal axis.

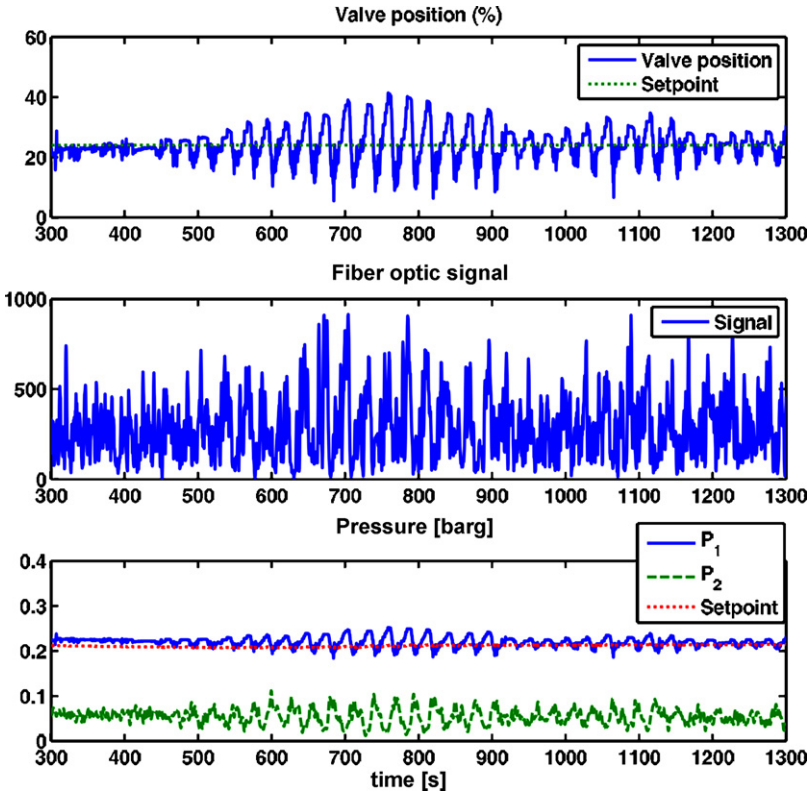

Fig. A1 – Control quality when setpoint outer loop is 24%.

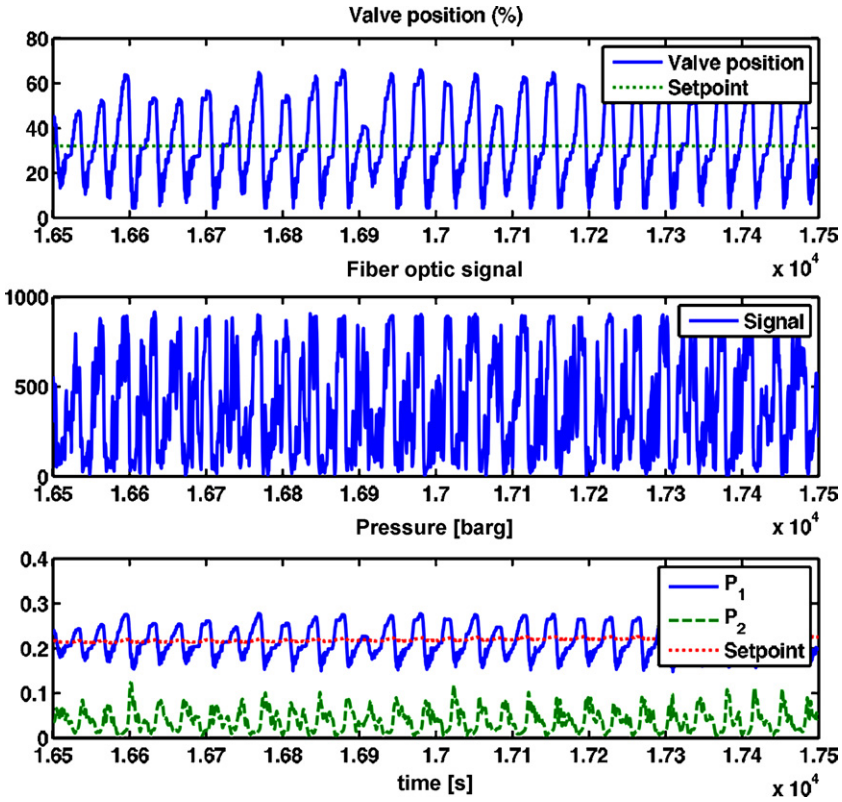

Fig. A2 – Control quality when setpoint outer loop is 32%.

A.3. *Tuning procedure*

The model parameters K_1 in the choke valve equation, K_2 in the expression for internal gas velocity (A.8) and K_3 and the exponent n in the entrainment model (Eqs. (A.9) and (A.11)) are the four free parameters (degrees of freedom) that can be used to tune the model. In addition to these four empirical coefficients, some of the physical parameters that have been assumed to be constant in the model are varying in the real system, and the values for these parameters can also be used as tuning parameters. These physical parameters include the average molecular weight of the gas, M_G, and the upstream gas volume, V_{G1}. These physical parameters are not regarded as degrees of freedom as they are only used to fine-tune the model.

The tuning of the model will depend on the available data. Accurate field data for the real system is obviously the best alternative, but this is rarely available. The easiest way to obtain the data needed is generate them from a more detailed model, often built in a commercial simulator such as OLGA, which is tuned to give a reasonably accurate description of the system. This approach can provide data over a wide range of operating conditions and valve openings without the prohibiting costs associated with field test.

Our tuning strategy will be to identify the bifurcation point from the reference data and use two measurements (for example the upstream pressure P_1 and the topside pressure P_2) to fix two degrees of freedom in the stationary solution of the model. Fixing the stationary value of h_1 in the interval $0 < h_1 < H_1$ allows us to find K_1, K_2, K_3 and n from the stationary solution of the model. Finally, the physical properties M_G and V_{G1} as well as the value used for h_1 can be adjusted to get an acceptable fit of pressure levels, amplitudes, and frequencies for other valve openings.

Note that due to the lumped nature of the model, we cannot model the variations in parameters in the feed section of the pipeline. This means that we can only tune the model to data from a specified point in the feed pipeline, variations along the feed pipeline is not included.

Appendix B. Experimental results

Figures showing the behavior when increasing the set point, z_s for the outer loop using measurement P_1 in the inner loop: Figs. A1 and A2.

References

Baardsen, I. Slug regulering i tofase strømning - eksperimentell verifikasjon, November 2003.

Barnea, D., 1987, A unified model for predicting flow pattern transitions for the whole range of pipe inclinations. Int. J. Multiphase Flow, 13: 1–12.

Chen, J., 2000, Logarithmic integrals, interpolation bounds and performance limitations in MIMO feedback systems. IEEE Trans. Autom. Control, AC-45(6): 1098–1115.

Courbot, A., 1996, Prevention of severe slugging in the Dunbar 16″ multiphase pipeline, In *Offshore Technology Conference* May 6–9, Houston, TX,

Godhavn, J.M., Fard, M.P. and Fuchs, P.H., 2005, New slug control strategies, tuning rules and experimental results. J. Process Control, 15(15): 547–577.

Havre, K. and Skogestad, S., 2002, Achievable performance of multivariable systems with unstable zeros and poles. Int. J. Control, 74: 1131–1139.

Havre, K., Stornes, K.O. and Stray, H., 2000, Taming slug flow in pipelines. ABB Rev., 4(4): 55–63.

Hedne, P. and Linga, H., 1990, Suppression of terrain slugging with automatic and manual riser choking. Adv. Gas–Liquid Flows, 453–469.

Hewitt, G.F. and Roberts, D.N. Studies of two-phase flow patterns by simultaneous X-ray and flash photography. Technical report, UKAEA Report AERE M-2159, 1969.

Hollenberg, J.F., de Wolf, S. and Meiring, W.J., 1995, A method to suppress severe slugging in flow line riser systems. Oil Gas J.,

Schmidt, Z., Brill, J.P. and Beggs, H.D., 12 1979, Choking can eliminate severe pipeline slugging. Oil Gas J., (12): 230–238.

Schmidt, Z., Brill, J.P. and Beggs, H.D., 1980, Experimental study of severe slugging in a two-phase pipelineriser system. Soc. Petrol. Engrs. J., 407–414. SPE 8306

Sivertsen, H. and Skogestad, S., 2005, Anti-slug control experiments on a small scale two-phase loop, In *ESCAPE' 15* Barcelona, Spain, 29 May to 1 June,

Sivertsen, H., Alstad, V., and Skogestad, S. Medium scale experiments on stabilizing riser slug flow, SPE Projects, Facilities & Construction, In Press, 2009.

Skofteland, G. and Godhavn, J.M., 2003, Suppression of slugs in multiphase flow lines by active use of topside choke—field experience and experimental results, In *Proceedings of multiphase '03* San Remo, Italy, 11–13 June 2003,

Skogestad, S. and Postlethwaite, I., (1996). *Multivariable Feedback Control.* (John Wiley & Sons).

Storkaas, E., Skogestad, S. and Godhavn, J.M., 2003, A lowdimensional model of severe slugging for controller design and analysis, In *Proceedings of Multiphase '03* San Remo, Italy, 11–13 June 2003,

Storkaas, E. and Skogestad, S., 2007, Controllability analysis of two-phase pipeline–riser systems at riser slugging conditions. Control Eng. Pract., 15: 567–581.

Taitel, Y., 1986, Stability of severe slugging. Int. J. Multiphase Flow, 12(2): 203–217.

Taitel, Y. and Dukler, A.E., 1976, A model for predicting flow regime transitions in horizontal and near-horizontal gas–liquid flow. AIChE J., 22: 47–55.

Taitel, Y., Barnea, D. and Dukler, A.E., 1980, Modeling flow pattern transitions for steady upward gas–liquid flow in vertical tubes. AIChE J., 26: 345–354.

Zuber, N. and Findlay, J., 1965, Average volumetric concentration in two-phase flow systems. J. Heat Trans, 87: 453–468.